

# Anomalous Hall Effect in ZrTe<sub>5</sub>

Tian Liang<sup>1</sup>, Quinn Gibson<sup>2</sup>, Minhao Liu<sup>1</sup>, Wudi Wang<sup>1</sup>, R. J. Cava<sup>2</sup>, and N. P. Ong<sup>1</sup>  
*Departments of Physics<sup>1</sup> and Chemistry<sup>2</sup>, Princeton University, Princeton, NJ 08544*

(Dated: October 31, 2021)

ZrTe<sub>5</sub> has attracted considerable attention recently and whether it is Dirac/Weyl semimetal or not is now under intense discussion. Here, we performed in-situ 3D double-axes rotation to extract the full angular dependence of the transport properties. Clear anomalous Hall effect (AHE) was detected for every sample, with no magnetic ordering observed in the system under experimental resolution, revealed by the torque magnetometry. Interestingly, the AHE takes large values when the magnetic field is rotated in-plane, with the values vanishing above  $\sim 60$  K where the negative longitudinal magnetoresistance (MR) disappears, suggestive of the close relation in their origins, coming from Berry curvature generated by the Weyl nodes.

PACS numbers:

The notion of topology has been one of the central topics in condensed matter physics. ZrTe<sub>5</sub> has crystal structure of the orthorhombic layered structure with space group Cmcm ( $D_{2h}^{17}$ ) [1], as shown in the inset of Fig. 1A. The triangle prisms connecting Zr ions and three Te ions (depicted as the red dashed lines) form 1D chains of ZrTe<sub>3</sub> running along *a*-axis. These ZrTe<sub>3</sub> chains are connected by other Te ions which also form zigzag chains along *a*-axis and extend along *c*-axis. As a result, they form 2D layers and such 2D layers stack along *b*-axis via Van der Waals interaction to form the 3D crystal. The Van der Waals interaction along *b*-axis is very small with its value comparable to graphite [1]. Therefore, both the 2D single layer and the 3D bulk crystals of ZrTe<sub>5</sub> are of interest. The mono-layer of ZrTe<sub>5</sub> is theoretically predicted to be the quantum spin Hall (QSH) state and the 3D bulk ZrTe<sub>5</sub> is predicted to lie near the boundary of weak topological insulator (WTI) and strong topological insulator (STI) [1]. In our experiments, the 3D bulk crystals are studied.

ZrTe<sub>5</sub> has recently attracted considerable attention following the observation of negative longitudinal magnetoresistance (MR) [2], whose origin is claimed to come from the chiral anomaly [3–5], reminiscent of Dirac/Weyl semimetals [6–8]. However, unlike Na<sub>3</sub>Bi [9] and Cd<sub>3</sub>As<sub>2</sub> [10], there is so far no theoretical prediction showing that the system of ZrTe<sub>5</sub> is 3D Dirac semimetal protected by crystalline symmetries. Furthermore, the results of angle-resolved photoemission spectroscopy (ARPES) measurements so far are not converging yet [2, 11–14].

Therefore, it is intriguing to investigate the transport properties of ZrTe<sub>5</sub>, especially the anomalous Hall effect (AHE). The expression for the AHE of Dirac/Weyl semimetals reads as follows, viz.,

$$\sigma_{\text{AHE}} = e^2/h \left| \sum \Delta \mathbf{k}_i \right| \quad (1)$$

with  $\Delta \mathbf{k}_i$  representing the separation between the monopoles and anti-monopoles (Weyl nodes) in  $\mathbf{k}$ -space. Full angular dependence of the Hall signals were obtained to extract the AHE by in-situ 3D double axes rotation measurements.

Transport properties of ZrTe<sub>5</sub> are investigated with the current applied along the chain axis (*a*-axis). Fig. 1A shows the curves of resistivity versus temperature for selected samples showing that the resistivity increases down to the lowest temperatures where it starts to saturate. The resistivity versus temperature curves in the literatures [15, 16] show resistivity profiles with maximum peak sitting at  $T = T_0$ . The value of  $T_0$  varies between literatures and can take say  $T_0 = 135$  K [17] or 65 K [2]. It has been shown that the values of  $T_0$  can be systematically lowered to low temperatures via chemical pressure induced by substitution of rare earth elements [16]. Our samples can be regarded as the situation of  $T_0 \sim 5$  K. Although the resistivity increases as the temperature decreases, the value at 5 K is only  $\lesssim 5$  m $\Omega$  cm, so the system is still in the (bad) metallic regime. Since our interest is the AHE coming from the Berry curvature generated from Weyl nodes, it is worth checking that the AHE is not induced by the conventional mechanism like the ferromagnetism. For this purpose, we have performed torque magnetometry measurements whose results are shown in Fig. 1B for selected samples, with no magnetic ordering observed, confirming that the AHE in ZrTe<sub>5</sub> shown in Figs. 2, 3, 4, 5 (see below) are not coming from the ordinary mechanism induced by the ferromagnetism. This is a natural observation considering that ZrTe<sub>5</sub> consists of no magnetic elements.

The first clue that implies the existence of Berry curvature in the system coming from Weyl nodes originates from the observation of the anomalous Hall signals in *ab*-plane which is shown in Fig. 2. As shown in Fig. 2A, the negative longitudinal MR are narrowly confined  $\lesssim 1^\circ$ , reproducing the results obtained in Ref. [2]. Interestingly, the Hall signals show sharp zigzag shaped profile as shown in Fig. 2B, suggestive of the existence of the AHE emerging from the Weyl nodes. In order to extract the contribution from the Berry curvature, we have subtracted the linear background at high fields and plotted the anomalous part in panel D. The angular dependence of the magnitude of the anomalous Hall contribution as plotted in panel C shows that the Berry curvature develops rapidly as soon as the magnetic field is tilted away

from the  $a$ -axis, indicative of the sharp sensitivity of the Weyl nodes to the direction of applied magnetic fields. It is clear from Fig. 2 that the amplitude of the anomalous contribution is not symmetric with respect to the angle for sample Z2. This suggests that the AHE has additional component which emerges from the in-plane component of the magnetic field which was not cancelled completely due to the slight misalignment.

In order to extract the contribution to AHE from the in-plane magnetic field as well as separate its contribution from the out-of-plane component, double axes rotator is employed to obtain the in-situ 3D full angular dependence of the anomalous Hall signals, which is plotted as a function of two angles,  $\varphi$  and  $\theta$ , respectively representing the azimuth and elevation angle, as shown in Fig. 3 for sample ZQ3. Panels j, k, l of Fig. 3 show the spherical plot of the anomalous Hall component, with the radius representing the magnitude of the anomalous Hall signals. When carefully aligned using double axes rotator, the out-of plane ( $ab$ -plane) anomalous Hall signals show completely antisymmetric behavior with respect to the  $a$ -axis as shown in panels a, b, c.

Next, we pay attention to the contribution coming from the in-plane ( $ac$ -plane) magnetic field. Remarkably, big sharp in-plane anomalous Hall signals are observed for every angle except when the magnetic field is parallel to  $a$ -axis as shown in panels d, e, f. The anomalous Hall contribution now has less sensitivity to the angle compared to the case of  $ab$ -plane with the anomalous Hall amplitude saturating only gradually as the angle increases. The in-plane Hall effect is quite anomalous, as the conventional Lorentz force cannot give any Hall signals. Yet, the experimental results show that there is large contribution of AHE, comparable or even larger than that coming from out-of plane ( $ab$ -plane), suggestive of contribution of Weyl nodes.

When the magnetic field is rotated in  $bc$ -plane, however, the contribution from the out-of plane ( $ab$ -plane) and in-plane ( $ac$ -plane) mix with each other and the AHE shows mixed behavior as shown in panels g, h, i. Interestingly, if the anomalous Hall signals are antisymmetrized with respect to the angle (curve in dark cyan in panel i), they give similar results as obtained for the case of out-of plane rotation ( $ab$ -plane). This suggests that the contribution from the  $b$ -axis can be simply obtained as the projection of the magnetic field onto the  $b$ -axis. By contrast, the in-plane ( $ac$ -plane) contribution cannot be obtained by the simple symmetrization process (curve in olive in panel i). Hence the magnetic field cannot simply

be thought as the projection onto the  $c$ -axis to reproduce the results. This infers that there might be two kinds of monopole anti-monopole pairs (Weyl nodes) which respond differently to the external magnetic fields.

In order to further test that the anomalous Hall effect is coming from the Weyl nodes, temperature dependence of the AHE is investigated which is shown in Fig. 4. As is clear from panel A, the negative longitudinal MR, suggestive of the chiral anomaly coming from the Weyl nodes, starts to become prominent below  $\sim 60$  K. The anomalous Hall signal shows similar trend which is clear from panel B, becoming substantial below  $\sim 60$  K. This implies the close relationship between the negative longitudinal MR and the AHE, confirming further that the origin of AHE is coming from the Weyl nodes.

We briefly discuss the results of the anomalous Nernst effect (ANE) shown in Fig. 5. Since the AHE is observed for  $\text{ZrTe}_5$ , it is natural to expect that the system also shows the ANE. One advantage of the Nernst effect is that the sensitivity is higher than the Hall signals [18–20]. Fig. 5 shows the angular dependence of the AHE and ANE for sample Z5. The close relation imply the same origin between the AHE and the ANE, coming from the Berry curvature induced by the Weyl nodes.

In conclusion, clear AHE develops for every sample under both in-plane ( $ac$ -plane) and out-of plane ( $ab$ -plane) magnetic fields. This AHE emerges at the same temperature where the negative longitudinal MR evolves, implying the same origin between them. Combined with the observation of torque magnetometry showing that no magnetic ordering develops in  $\text{ZrTe}_5$ , this suggests the existence of Weyl nodes in the system. The observation of sharp ANE further strengthens this claim. However, there is so far no clear evidence of ARPES measurements or theoretical predictions showing that the Weyl nodes exist in  $\text{ZrTe}_5$ . One thing that is worth noting, however, is that since  $\text{ZrTe}_5$  is located near the boundary of WTI and STI [1], if the inversion symmetry is broken in the system, then the system automatically falls into the Weyl semimetallic phase according to the general phase diagram proposed by Murakami *et al.* [6, 7, 21, 22]. Because the inversion symmetry broken Weyl states contains at least four Weyl nodes, or two pairs of monopoles and anti-monopoles, it would be interesting to investigate how they respond to the applied magnetic field. Investigating whether the inversion symmetry is broken in  $\text{ZrTe}_5$  as well as how the Weyl nodes appear are interesting directions to pursue in the future.

---

[1] Weng, H., Dai, X. & Fang, Z. Transition-Metal Pentatelluride  $\text{ZrTe}_5$  and  $\text{HfTe}_5$ : A Paradigm for Large-Gap Quantum Spin Hall Insulators. *Phys. Rev. X* **4**, 011002 (2014).  
 [2] Li, Q. *et al.* Chiral magnetic effect in  $\text{ZrTe}_5$ . *Nat Phys* **12**, 550–554 (2016).

[3] Adler, S. L. Axial-Vector Vertex in Spinor Electrodynamics. *Phys. Rev.* **177**, 2426–2438 (1969).  
 [4] Bell, J. S. & Jackiw, R. A PCAC puzzle:  $\pi^0 \rightarrow \gamma\gamma$  in the  $\sigma$ -model. *Il Nuovo Cimento A (1971-1996)* **60**, 47–61 (1969).  
 [5] Nielsen, H. & Ninomiya, M. A no-go theorem for reg-

- ularizing chiral fermions. *Physics Letters B* **105**, 219 – 223 (1981).
- [6] Murakami, S. & Kuga, S.-i. Universal phase diagrams for the quantum spin Hall systems. *Phys. Rev. B* **78**, 165313 (2008).
- [7] Okugawa, R. & Murakami, S. Dispersion of Fermi arcs in Weyl semimetals and their evolutions to Dirac cones. *Phys. Rev. B* **89**, 235315 (2014).
- [8] Hosur, P. & Qi, X. Recent developments in transport phenomena in Weyl semimetals. *Comptes Rendus Physique* **14**, 857 – 870 (2013).
- [9] Wang, Z. *et al.* Dirac semimetal and topological phase transitions in  $A_3\text{Bi}$  ( $A = \text{Na}, \text{K}, \text{Rb}$ ). *Phys. Rev. B* **85**, 195320 (2012).
- [10] Wang, Z., Weng, H., Wu, Q., Dai, X. & Fang, Z. Three-dimensional Dirac semimetal and quantum transport in  $\text{Cd}_3\text{As}_2$ . *Phys. Rev. B* **88**, 125427 (2013).
- [11] Wu, R. *et al.* Evidence for Topological Edge States in a Large Energy Gap near the Step Edges on the Surface of  $\text{ZrTe}_5$ . *Phys. Rev. X* **6**, 021017 (2016).
- [12] Zhang, Y. *et al.* Electronic Evidence of Temperature-Induced Lifshitz Transition and Topological Nature in  $\text{ZrTe}_5$ . *ArXiv e-prints* (2016). arXiv:1602.03576.
- [13] Manzoni, G. *et al.* Ultrafast Optical Control of the Electronic Properties of  $\text{ZrTe}_5$ . *Phys. Rev. Lett.* **115**, 207402 (2015).
- [14] Hongyu Xiong *et al.* *Unpublished*.
- [15] Littleton, R. T. *et al.* Effect of Ti substitution on the thermoelectric properties of the pentatelluride materials  $\text{M}_{1-x}\text{Ti}_x\text{Te}_5$  ( $\text{M}=\text{Hf}, \text{Zr}$ ). *Applied Physics Letters* **72**, 2056–2058 (1998).
- [16] Lowhorn, N. D., Tritt, T. M., Abbott, E. E. & Kolis, J. W. Effect of rare earth doping on the thermoelectric and electrical transport properties of the transition metal pentatelluride  $\text{HfTe}_5$ . In *ICT 2005. 24th International Conference on Thermoelectrics, 2005.*, 41–45 (2005).
- [17] Fuller, W. *et al.* Pressure Effects in  $\text{HfTe}_5$  and  $\text{ZrTe}_5$ . *Journal de Physique* **44**, 1709–1712 (1983).
- [18] Behnia, K., Méasson, M.-A. & Kopelevich, Y. Oscillating Nernst-Ettingshausen Effect in Bismuth across the Quantum Limit. *Phys. Rev. Lett.* **98**, 166602 (2007).
- [19] Zhu, Z., Fauqué, B., Fuseya, Y. & Behnia, K. Angle-resolved Landau spectrum of electrons and holes in bismuth. *Phys. Rev. B* **84**, 115137 (2011).
- [20] Zhu, Z. *et al.* Quantum Oscillations, Thermoelectric Coefficients, and the Fermi Surface of Semimetallic  $\text{WTe}_2$ . *Phys. Rev. Lett.* **114**, 176601 (2015).
- [21] Murakami, S. Phase transition between the quantum spin Hall and insulator phases in 3D: emergence of a topological gapless phase. *New Journal of Physics* **9**, 356 (2007).
- [22] Murakami, S. Gap closing and universal phase diagrams in topological insulators. *Physica E: Low-dimensional Systems and Nanostructures* **43**, 748 – 754 (2011). NanoPHYS 09 Proceedings of the International Symposium on Nanoscience and Quantum Physics.

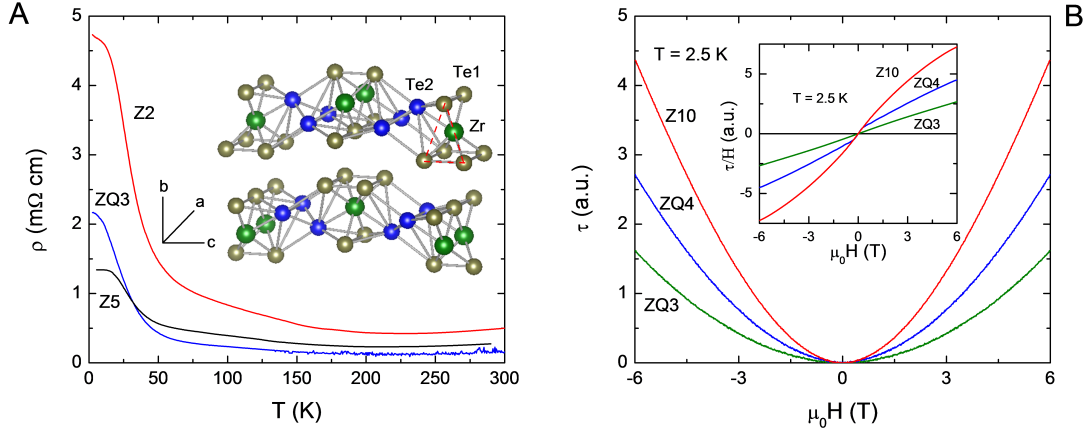


FIG. 1: Panel A: Resistivity as a function of temperature for selected samples. The resistivity decreases as the system cools down at high temperatures before it increases rapidly and saturates eventually at low temperatures. The inset shows the crystal structure of  $\text{ZrTe}_5$ . The triangle prisms connecting Zr ions and Te1 ions (depicted as the red dashed lines) form 1D chains running along a-axis. Te2 ions, also forming zigzag chains along a-axis, extend along c-axis to connect  $\text{ZrTe}_3$  chains, making 2D layers. These 2D layers stack along b-axis via Van der Waals interaction to form the 3D crystal. Panel B: Torque magnetometry data as a function of magnetic field for selected samples at 2.5 K. The inset shows  $\tau/H$  (torque divided by magnetic field). The torque  $\tau$  shows  $\sim$  quadratic behavior, implying the dominant contribution is either paramagnetic or diamagnetic response.  $\tau/H$  has no anomaly at low fields except for sample ZQ4, implying no magnetic order. For sample ZQ4, although small anomaly is found for  $\tau/H$  below  $\sim 0.3 \text{ T}$ , the onset of the AHE is  $\gtrsim 1 \text{ T}$ , so their origins are different. Furthermore, while every sample shows AHE, not all samples show the anomaly, again implying the different origins between them.

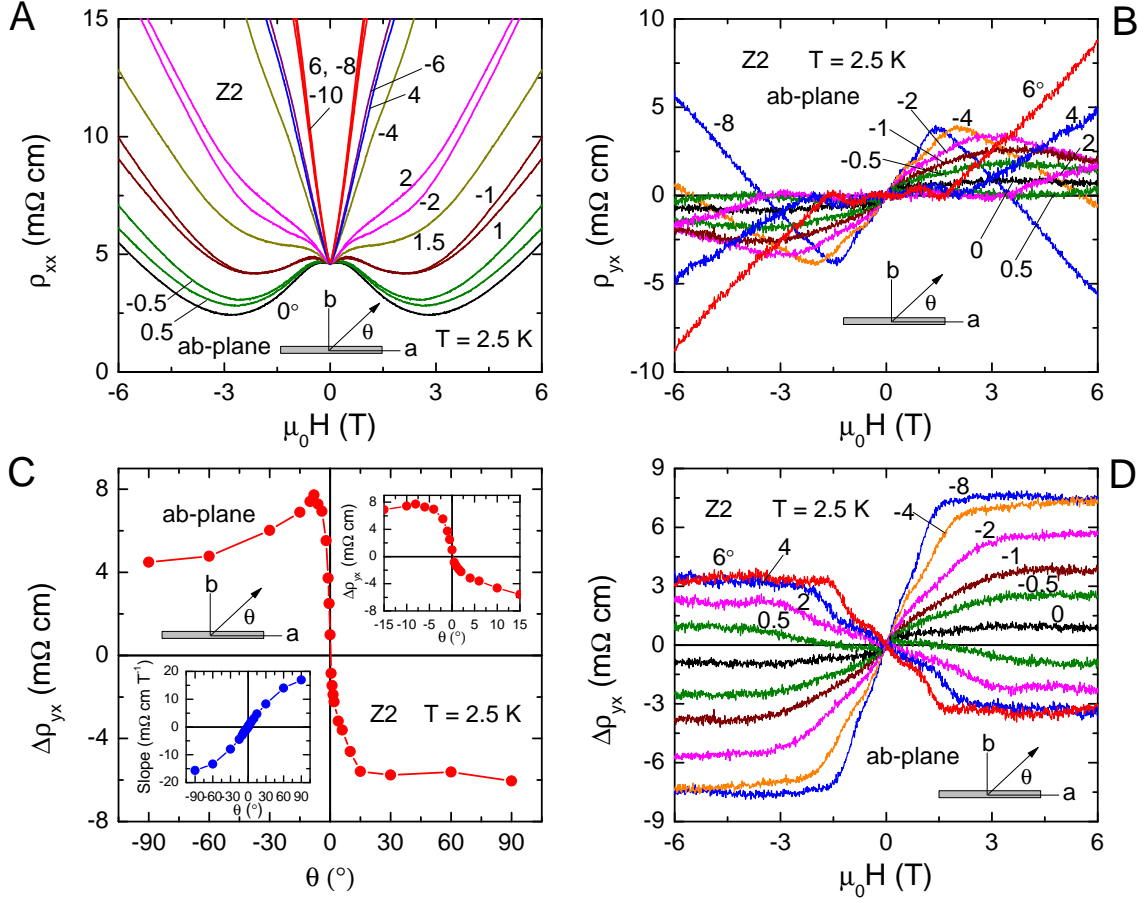


FIG. 2: Angular dependence of MR and Hall at selected angles in ab-plane. Panel A: Negative longitudinal MR is observed in small angle regime  $\theta \lesssim 1^\circ$ . Panel B: Hall signals show zigzag shape manifesting the existence of anomalous Hall contribution. Panel C: Full angular dependence of the anomalous Hall amplitude obtained from Panel D. The right top inset shows the anomalous Hall amplitude at small angles and the left lower inset shows the angular dependence of the background slope. Panel D: Anomalous Hall signals after linear background subtraction from Panel B.

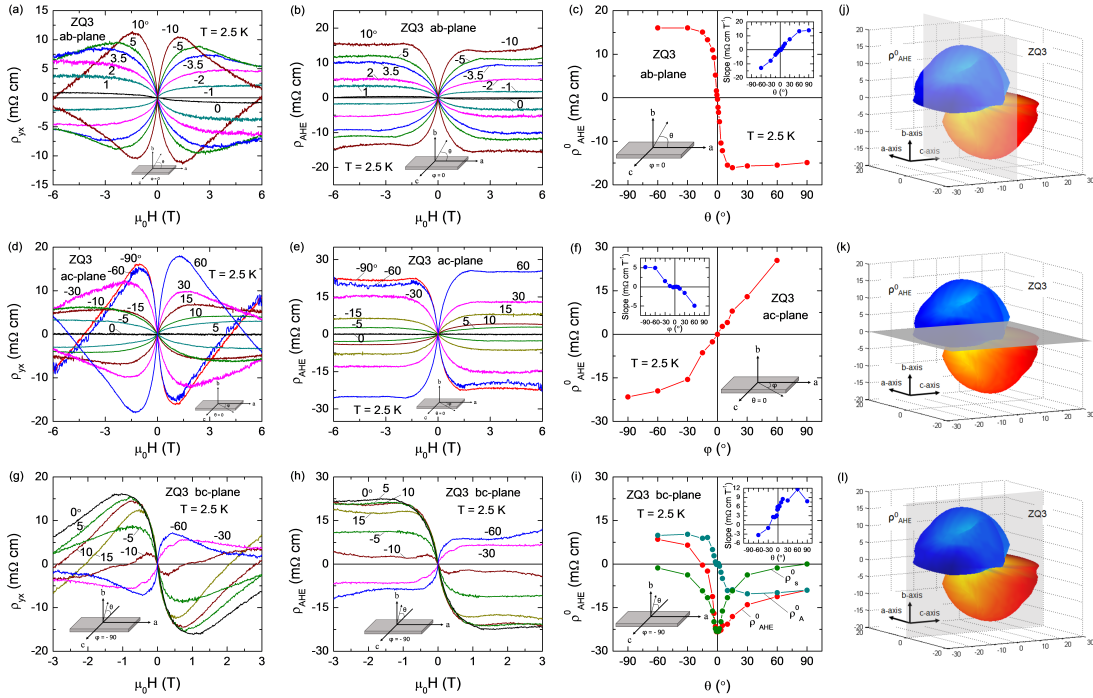


FIG. 3: Full 3D angle dependence of the AHE  $\rho_{\text{AHE}}^0$  investigated for sample ZQ3. When the magnetic field is rotated in  $ab$ -plane (out of plane), sharp anomalous Hall signals are observed with the Berry curvature saturating rapidly as the magnetic field tilts away from  $a$ -axis (panels a, b, c). When the magnetic field is rotated instead in  $ac$ -plane (in-plane), comparable or even larger anomalous Hall signals are observed, now with the Berry curvature less sensitive to the direction of the magnetic field (panels d, e, f). When the magnetic field is rotated in  $bc$ -plane (panels g, h, i), the system picks up the mixed contribution of anomalous Hall signals showing tilted behavior of the Berry curvature as a function of angle as shown in panel i. The antisymmetrized contribution  $\sigma_A^0$  shown as the curve in dark cyan resembles the Berry curvature obtained for  $ab$ -plane. By contrast, the symmetrized contribution  $\sigma_S^0$  does not follow the profile shown in panel f for the case of  $ac$ -plane, inferring that there might exist two different types of monopoles anti-monopoles (Weyl nodes) in the system. Panels j, k, l show the 3D spherical plot of the anomalous Hall signal  $\rho_{\text{AHE}}^0$ , with the blue color representing the negative value and orange showing the positive value. The principal planes are also shown for clarity.

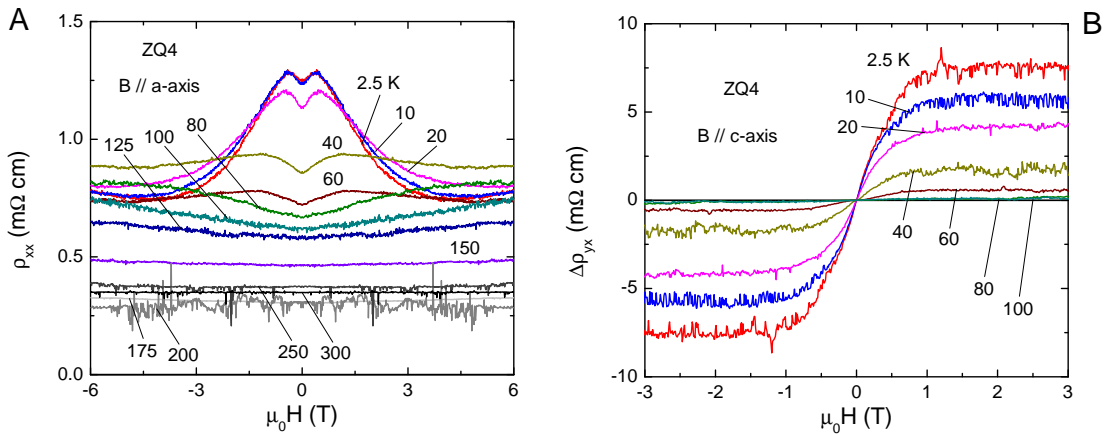


FIG. 4: Temperature dependence of MR and Hall signals. Panel A: The negative longitudinal MR starts to grow rapidly below  $\sim 60$  K. Panel B: Correspondingly, the anomalous Hall signals become prominent below  $\sim 60$  K, showing close relation between the negative longitudinal MR and the anomalous Hall effect.

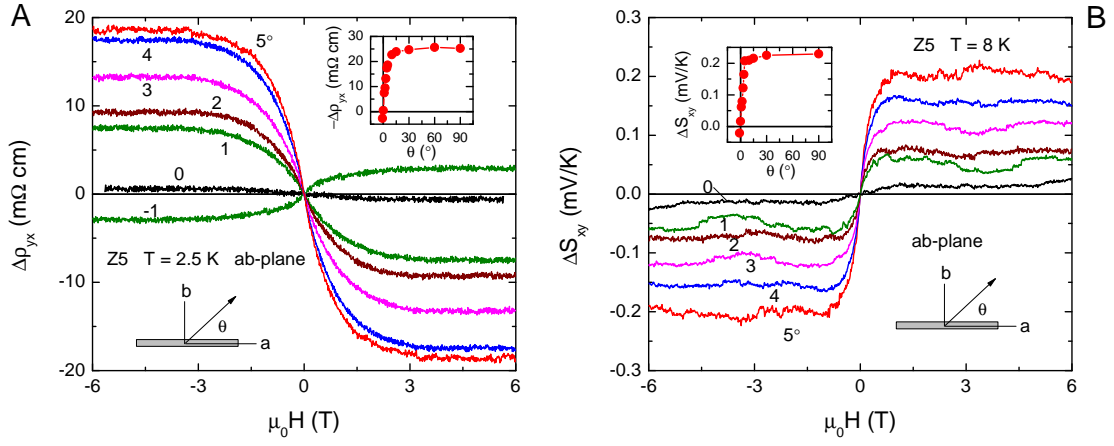


FIG. 5: Angular dependence of anomalous Hall (panel A) and Nernst (panel B) signals at small angles. The insets show the angular dependence of the amplitude of the anomalous signals. The close similarity between the anomalous Hall and Nernst effect suggests the same origin of both signals.